Diffusion tensor imaging in biomechanical studies of skeletal muscle function

C. C. VAN DONKELAAR[1], L. J. G. KRETZERS[3], P. H. M. BOVENDEERD[3], L. M. A. LATASTER[2], K. NICOLAY[4], J. D. JANSSEN[3,1] AND M. R. DROST[1,3]

[1] *Department of Movement Sciences, Cardiovascular Research Institute Maastricht (Carim),* [2] *Department of Anatomy and Embryology, Maastricht University,* [3] *Department of Mechanical Engineering, Technical University Eindhoven,* [4] *Bijvoet Center, Utrecht University, The Netherlands*

(*Accepted 30 September 1998*)

ABSTRACT

In numerical simulations of skeletal muscle contractions, geometric information is of major importance. The aim of the present study was to determine whether the diffusion tensor imaging (DTI) technique is suitable to obtain valid input with regard to skeletal muscle fibre direction. The accuracy of the DTI method was therefore studied by comparison of DTI fibre directions in the rat tibialis anterior muscle with fascicle striation patterns visible on high-resolution magnetic resonance imaging (MRI) and with fibre directions in an actual longitudinal section (ALS) through the same muscle. The results showed an excellent qualitative agreement between high-resolution MRI and DTI. Despite less accurate quantitative comparison with ALS, it was concluded that DTI does indeed measure skeletal muscle fibre direction. After the experiment, it was possible to determine an appropriate voxel size (0.9 mm^3) that provided enough resolution and acceptable accuracy (5°) to use DTI fibre directions in biomechanical analyses. Muscle deformation during contraction, resulting from a finite element simulation with a mesh that was directly generated from the experimental data, has been presented.

Key words: MRI; muscle fibre orientation; finite element modelling.

INTRODUCTION

Biomechanical studies have shown that the mechanical behaviour of muscle depends strongly on muscle architecture (Bovendeerd et al. 1992, 1994; Van Leeuwen & Spoor, 1992). To analyse muscle mechanics and to calculate the distribution of mechanical properties such as stress and strain, accurate data regarding muscle fibre orientation are needed.

Traditional anatomical reconstruction techniques to determine 3D muscle fibre orientations have many disadvantages (McLean & Prothero, 1992). Two alternative methods, based on MRI, have been used previously: high-resolution (conventional) MRI and diffusion tensor imaging (DTI). In high-resolution MRI of skeletal muscle, a striation pattern is visible provided the image is coplanar with the fascicle orientation (Engstrom et al. 1991). Complete 3D reconstruction of fibre fields seems possible with this method (Scott et al. 1993), but a large number of planes is needed and fibre directions have to be determined from the images. DTI measurements are independent of the orientation of the image plane, and 3D fibre directions are obtained immediately.

The DTI technique is based on measurement of the apparent diffusion of water in a (biological) tissue. From a series of diffusion weighted images, employing diffusion sensitisation in 6 independent directions, a diffusion tensor can be calculated in each voxel (Basser et al. 1994*a*). The eigenvalues and eigenvectors of this tensor provide information about local tissue anisotropy. The eigenvector belonging to the largest eigenvalue of the diffusion tensor is assumed to coincide with the local muscle fibre direction in striated muscle (Basser et al. 1994*b*; Garrido et al. 1994; Hsu et al. 1998) and with the myelinated fibre

Correspondence to Dr C. C. van Donkelaar, Dept of Movement Sciences, Maastricht University, P.O. Box 616, 6200 MD Maastricht, The Netherlands, Tel: +31-433881398; fax: +31-433670972; e-mail: *rene.vandonkelaan@bw.unimaas.nl*

direction in brain white matter (Coremans et al. 1994; Moseley et al. 1990; Nakada & Matsuzawa, 1995; Pierpaoli & Basser, 1996). In the present paper, the direction of this eigenvector will be referred to as the DTI direction.

Qualitative resemblance between DTI directions and visual anatomy (Cleveland et al. 1976; Basser et al. 1994*b*; Van Doom et al. 1996) or essential features of cardiac architecture (Garrido et al. 1994; Reese et al. 1995; Hsu et al. 1998) have been described in the literature. Basser et al. (1994*b*) showed that the principle directions of diffusion co-rotated with the orientation of a meat sample in successive measurements. This demonstrates that they are intrinsic to the material, but not that they coincide with fibre directions. The only study with respect to the quantitative accuracy of the DTI technique attended cardiac muscle. DTI fibre orientation and histological slices showed distinctive correlation (Hsu et al. 1998). It is hypothesised that this holds for skeletal muscle as well as for cardiac muscle.

The first aim of the present study is to verify the hypothesis that DTI fibre orientation coincides with skeletal muscle fibre direction. Therefore, DT directions in the midsagittal plane of the tibialis anterior (TA) muscle of a rat were compared qualitatively with fascicle orientations that were visible in high-resolution MR images, and quantitatively with fibre directions measured in an actual longitudinal section through the same plane of that muscle. In addition, this study shows the practical use of the DTI method in biomechanical research on skeletal muscle functioning. The finite element (FE) method, which has become familiar in biomechanical research on skeletal and cardiac muscle behaviour (Vankan et al. 1991, 1998; Bovenderd et al. 1992; Huyghe et al. 1992), essentially makes use of geometric and spatial information. One major difficulty and time-consuming issue in such studies is to generate accurate FE meshes. Furthermore, in FE models of contracting skeletal muscle not only is the muscle geometry important, but simulations are also very sensitive to fibre directions. They may become unstable with large variations in fibre direction (too small voxel size) but become inappropriate if the fibre direction input is erroneous, for instance if the V-shaped fibre direction around an intramuscular aponeurosis is smoothed (too large voxel size).

The combination of high-resolution MRI and DTI provides a potential way of simplifying the creation of FE meshes for any kind of skeletal muscle. In the present study, the TA muscle contour was determined from a high-resolution MR image and an appropriate voxel size determined from the DTI data to incorporate DTI-determined muscle fibre directions in a FE model of contracting skeletal muscle. This was done by clustering original voxels to larger effective voxel sizes. An FE simulation of a tetanic contraction will illustrate the results.

MATERIALS AND METHODS

The left hind leg of an anaesthetised male Lewis rat (age 11 wk) was fixed at an ankle angle of 110° (slight plantar flexion) and a knee angle of 90°. After perfusion fixation with 5% buffered formalin, the left leg was dissected and the skin and part of the dorsal musculature were removed. The leg was fixed in a PVC tube (outer diameter 20 mm, inner diameter 17 mm) using polyurethane foam. A groove (depth 0.8 mm, width, 1.0 mm) with an increasing pitch was drilled in the outer surface of the tube and filled with ECG electrode gel. As this groove was visible in MR images and in the specimen, it served as an external reference system to link results. Two glass haematocrit capillaries (inner diameter 0.22 mm) were filled with tap water and glued to the outside of the tube at both sides of the estimated position of the midsagittal TA plane. In combination with MR images, these capillaries facilitated determination of the midsagittal TA plane.

MR images were obtained a 20 °C with a 4.7 T SISCO 200/400 system, operating at 200 MHz for protons and equipped with Oxford gradients (maximal gradient strength of 220 mT/m). On the basis of high resolution images, it was ensured that the x, y and z axes of the magnet coincided with the longitudinal (proximodistal), transverse (lateromedial), and sagittal (dorsoventral) muscle axes, respectively.

Diffusion was measured by incorporating pulsed gradients into a spin echo imaging sequence, according to Stejskal & Tanner (Stejskal & Tanner, 1965; Pierpaoli & Basser, 1996). Pulsed gradients were placed symmetrically around the 180° refocusing pulse. The readout gradient rephasing lobe was placed directly before the echo acquisition. Gradient strength was increased from 0 to 117 mT/m in 3 steps (i.e. 4 gradient strengths were applied), in each of the 6 directions: x, y, z, xy, xz and yz. Echo time equalled 35 ms, diffusion gradient pulse duration and separation were 7.5 and 15 ms respectively (Van Doorn et al. 1996).

For each voxel, an apparent diffusion coefficient in each of the 6 independent directions (x, y, z, xy, xz and yz) was calculated from the measured signal intensities

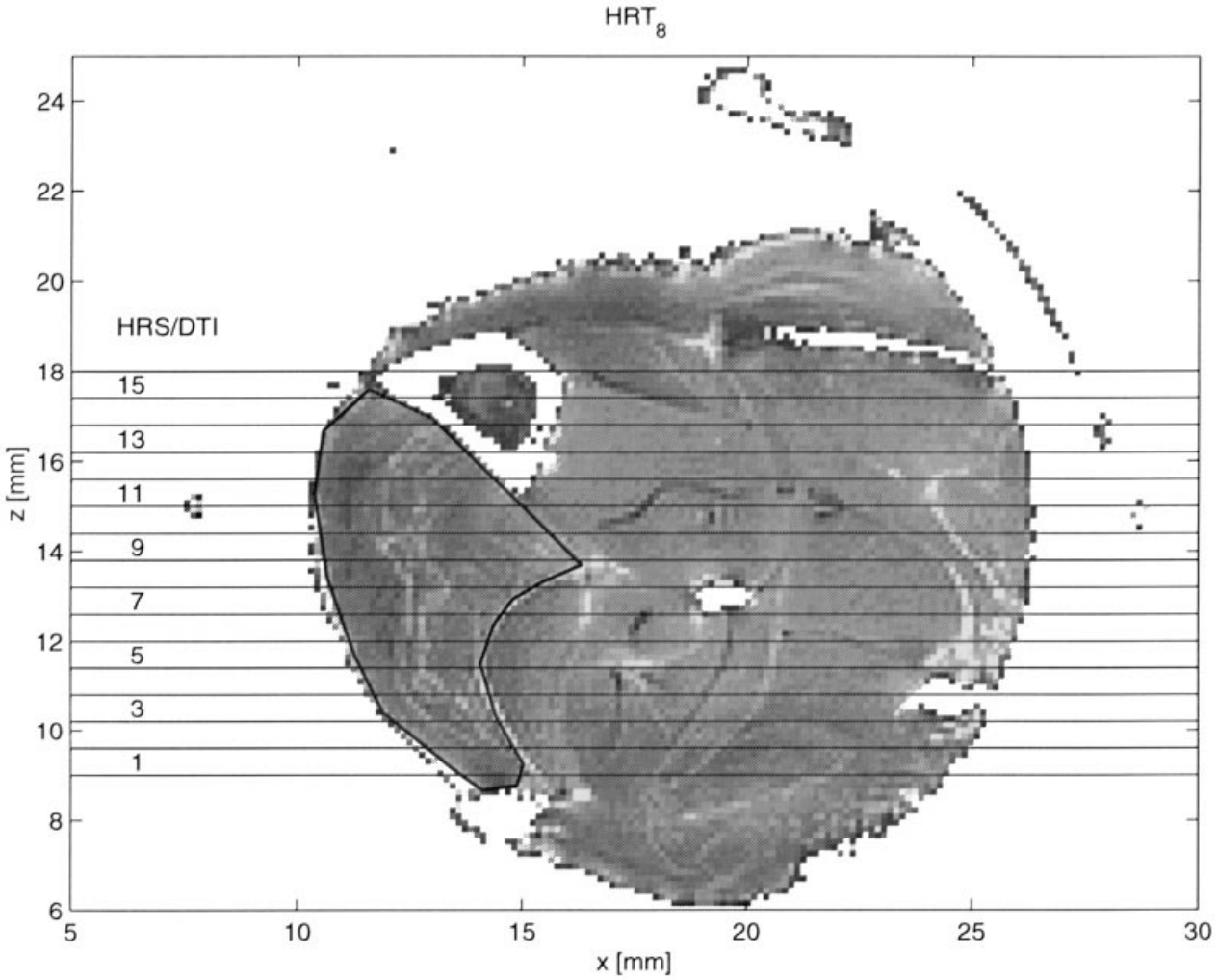

Fig. 1. Transverse high resolution image (HRT-8) halfway through the TA (orientation: left: ventral, bottom: lateral). The TA, roughly indicated by a thin white polygon, can clearly be seen just below the white semicircular tibia in the left upper part of the picture. Locations of the 15 HRS and the 15 DTI slices are indicated.

at 4 applied gradient strengths. Values based on a correlation between the natural logarithm of the relative signal intensity and the b value of less than 0.9 were excluded from further analysis. From the 6 diffusion coefficients, 1 for each of the 6 directions, diffusion tensors were obtained from which eigenvalues and eigenvectors per voxel were calculated. The eigenvalues were sorted in decreasing magnitude: $\lambda_1 > \lambda_2 > \lambda_3$. The eigenvector belonging to λ_1 is thought to represent the local muscle fibre direction and will therefore be referred to as the DTI direction. The above procedure has been described in more detail by Basser et al. (1994*a*).

High-resolution MR images of sagittal (HRS) and transverse (HRT) muscle planes (x–z and y–z plane of the MRI magnet), as well as DTI data of sagittal planes were obtained. DTI and HRS images were collected in 15 contiguous slices of 0.6 mm, in a field of view of 70∗35 mm². There was 1.4 mm distance between the 15 successive 0.6 mm thick HRT images, in a field of view of 35∗35 mm². Data matrix of HRS and HRT measurements was 256∗256, whereas DTI images consisted of 128∗128 pixels. Thus, DTI voxel size (x∗y∗z) equalled 0.55∗0.6∗0.27 = 0.090 mm³. The positions of all DTI and HRS planes are indicated in the HRT image through the thickest part of the TA muscle, as shown in Figure 1.

After the MRI experiment, the midsagittal plane of the specimen was found to coincide with slice 9 (Fig. 1), as determined from the external reference system and all high-resolution images. The midsagittal plane of the muscle is defined as the plane parallel to the sagittal plane of the body that includes the thickest part of the TA (see Fig. 1). The images that correspond to this plane will be referred to as HRS-9 (the midsagittal high resolution image) and DTI-9 (the

DTI image of the same plane). The specimen was sawn through this specific plane, using an Exakt diamond-coated band saw with a D64 sawing blade. Due to machining, the opposing surfaces in the sawing plane were approximately 0.4 mm apart. The medial surface of the 2 halves of the specimen resembled the HRS-9 image. This surface will be referred to as ALS (actual longitudinal section). Surface contrast of ALS was enhanced by 15 s staining with 0.2% toluidine blue. Muscle fibres were clearly visible on the exposed surfaces, except for a small area ventral to the distal aponeurosis. A photographic slide (Ektachrome 64) was made with a Nikon F501 camera and a micro Nikkor 105 mm lens. The contours of the TA, including its aponeuroses, as well as the positions of the reference frame, were traced from an $80*20\ cm^2$ projection with a Zeiss Unimat projector and a Zett Varioo Talon lens. A computer slide of HRS-9 was projected and traced in the same way. These tracings served as a basis to couple the frames of reference from ALS and MRI, to permit comparison of the fibre fields. ALS fibre angles on specific locations were determined from the projected slide, using a digitiser table (Summagraphics ID).

HRS-9, DTI-9 and ALS all provide information regarding local fibre directions. The fibre angle was defined as the angle between DTI or muscle fibre direction and the positive x direction (see Fig. 3 for the orientation of the axes). DTI-9 was compared qualitatively with HRS-9 by projecting unity vectors of the first eigenvectors of DTI-9 on that image. Quantitative comparison between ALS and DTI-9 was performed in 2 ways. Firstly, a distributed region of interest was defined as 29 positions within the TA, including the complete range of fibre directions in the ALS. As the fibre direction was not clearly visible in ALS in the area ventral to the distal aponeurosis, this region was excluded. The local ALS fibre directions in the distributed region of interest were measured. The error angle, defined as the angle between ALS and DTI-9, was calculated for each of the 29 locations. Secondly, another region of interest was defined in the TA, this being the proximal area in which muscle fibres run predominantly parallel. The average ALS fibre direction was measured, and the variation in fibre angles in this area was estimated from the ALS projection. In DTI, the proximal region of interest is the area between (39.7, 9.3) and (47.9, 13.4) in Figure 3*a* and contains 225 (15*15) DTI voxels. The mean DTI angle and its standard deviation were compared with the general ALS fibre direction in this area.

An approximate voxel size for the use of DTI muscle fibre directions in FE models was defined as the smallest voxel size that provides a standard deviation for the fibre directions of $< 5°$. To determine an appropriate DTI voxel size, new effective voxels of different sizes were defined within the previously mentioned proximal region of interest. These new voxels consisted of at least 4 voxels, the ratio of their sides being between 0.5 and 2 voxels. A new diffusion coefficient for each of the 6 directions was calculated per new voxel, this being the average diffusion coefficient of the original voxels within the new one. Averaging diffusion coefficients is identical to averaging the primary image data, since those are linearly related. From the averaged values, new DTI directions were calculated. The mean DTI direction and standard deviation of the new voxels within the proximal region of interest were calculated for each effective voxel size. Theoretically, the standard deviation would decrease by $n^{-0.5}$, where n is the number of original voxels per new voxel, whereas the mean DTI direction should not change.

To create the FE mesh to be used in the simulation of a muscle contraction, TA contours on the HRS-9 image were obtained by marking outline coordinates on the high resolution image in conjunction with close examination of the ALS under a stereomicroscope. From this contour, the program Sepview (Sepra Analysis, Leidschendam, The Netherlands) automatically generated the distribution of elements in this particular geometry. A local fibre direction was assigned to each element, which was calculated by averaging the DTI directions in the previously determined appropriate voxel size surrounding the element centre. A simulated tetanic contraction of the TA with these realistic fibre directions was performed using the finite element model of perfused contracting skeletal muscle recently described by Vankan et al. (1996, 1998).

RESULTS

The diffusion images of DTI-9 in the 6 directions x, y, z, xy, xz and yz are shown in Figure 2. Judging from the intensity of the diffusion image in the x direction, diffusion of water is easiest in that direction.

The HRS-9 image is shown in Figure 3*a*. The TA covers the area ventral to $z = 15$ mm almost completely. Its distal aponeurosis is clearly visible in this image as a dark line from coordinates (26, 13) to (36, 11). Muscle fascicles are visible as faint striations over approximately half of the muscle, dorsally less clear than ventrally. Note the pennate insertion of the fascicles on the distal aponeurosis. In Figure 3*b*, a projection of DTI-9 directions is superimposed on

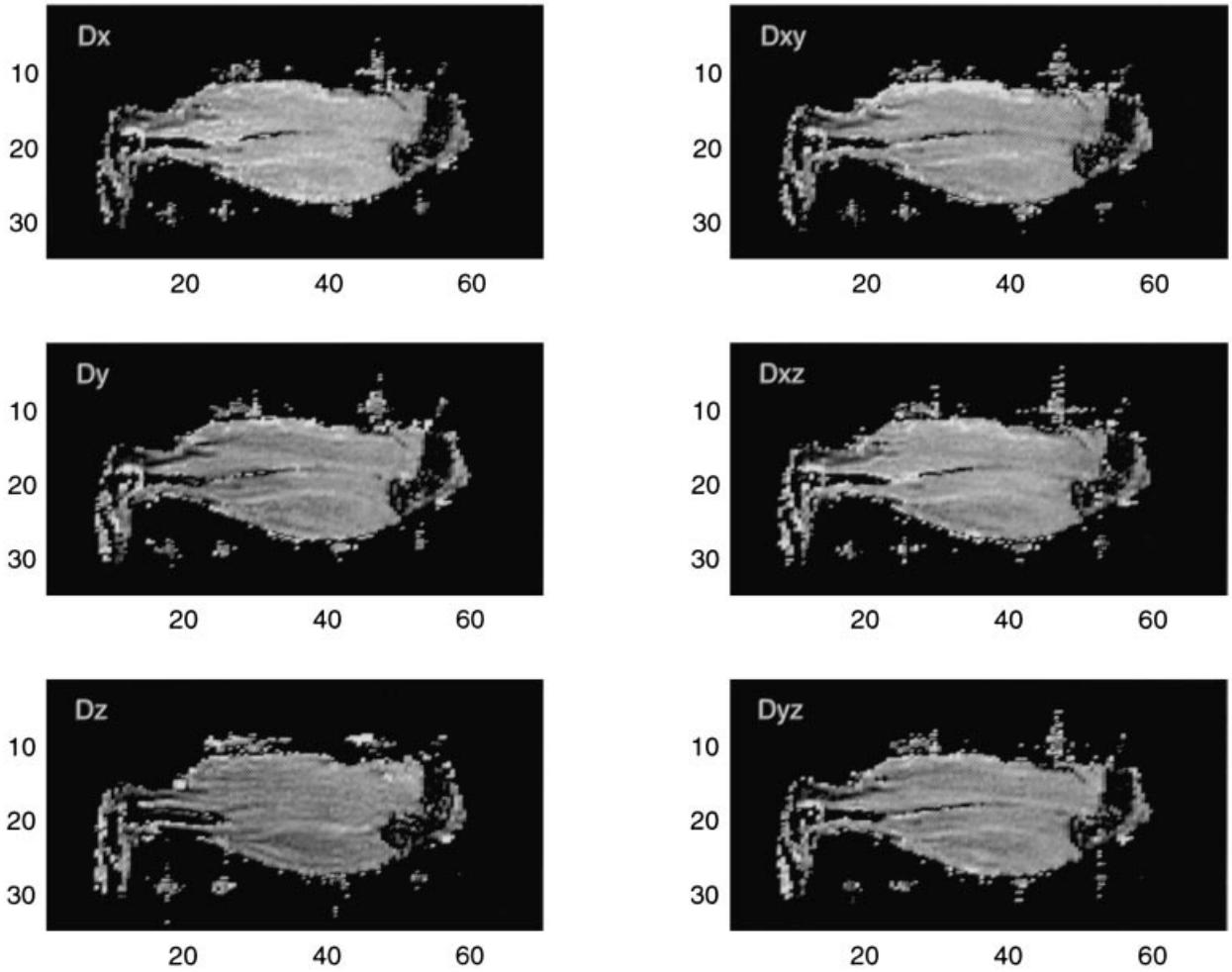

Fig. 2. Diffusion maps of the 6 directions Dx, Dy, Dz, Dxy, Dxz and Dyz of DTI-9. The corresponding high resolution image is shown in Fig. 3. Differences in pixel intensity between Dx, i.e. the expected predominant fibre direction and Dy/Dz, perpendicular to the fibre direction are obvious.

HRS-9. The DTI direction in each voxel in this image is based on averaged diffusion coefficients over 10 surrounding voxels. This image is an enlargement of the area around the distal aponeurosis in Figure 3*a*. Since the lines are 2D projections of 3D unit vectors, shorter lengths imply larger out-of-plane directions. The DTI directions follow the muscle fascicle direction visible as faint striations in HRS-9 quite well, and the pennate insertion of DTI directions on the distal aponeurosis is obvious. The outermost DTI directions along the ventral side of the TA are less ordered and do not follow the expected fibre direction. These voxels only partly contain muscle tissue, resulting in a lower signal to noise ratio in the original diffusion weighted images.

Table 1 shows the means and standard deviations of the 3 principal directions, the ratio between λ_1 and λ_3, and the trace of the diffusion tensor for the voxels in the distributed and the proximal region of interest. The large λ_1 with respect both to λ_2 and λ_3 reflects the strong transverse isotropic character of the tissue. The values correspond to those found in the literature (see Table 1), although our ratio λ_1/λ_3 is somewhat higher than that found in other studies.

The mean error angles and standard deviations (S.D.) between ALS and DTI-9 in the distributed region of interest are given in Table 2 for the original data and after averaging the diffusion coefficient over different numbers of voxels. At larger effective voxel sizes, error angles are significantly different from 0 ($P < 0.05$). In the proximal region of interest, the general ALS angle equals 0.3°, with an estimated variation due to a small gradient in this area of 2°. For each of the 125 possible combinations of effective voxel sizes in this area, a mean DTI direction was calculated. The mean value of these 125 mean DTI directions equals $-1.39° \pm 0.99°$. Thus ALS and DTI in the proximal region of interest differ by $\sim 1.7°$. The 125 S.D.s of

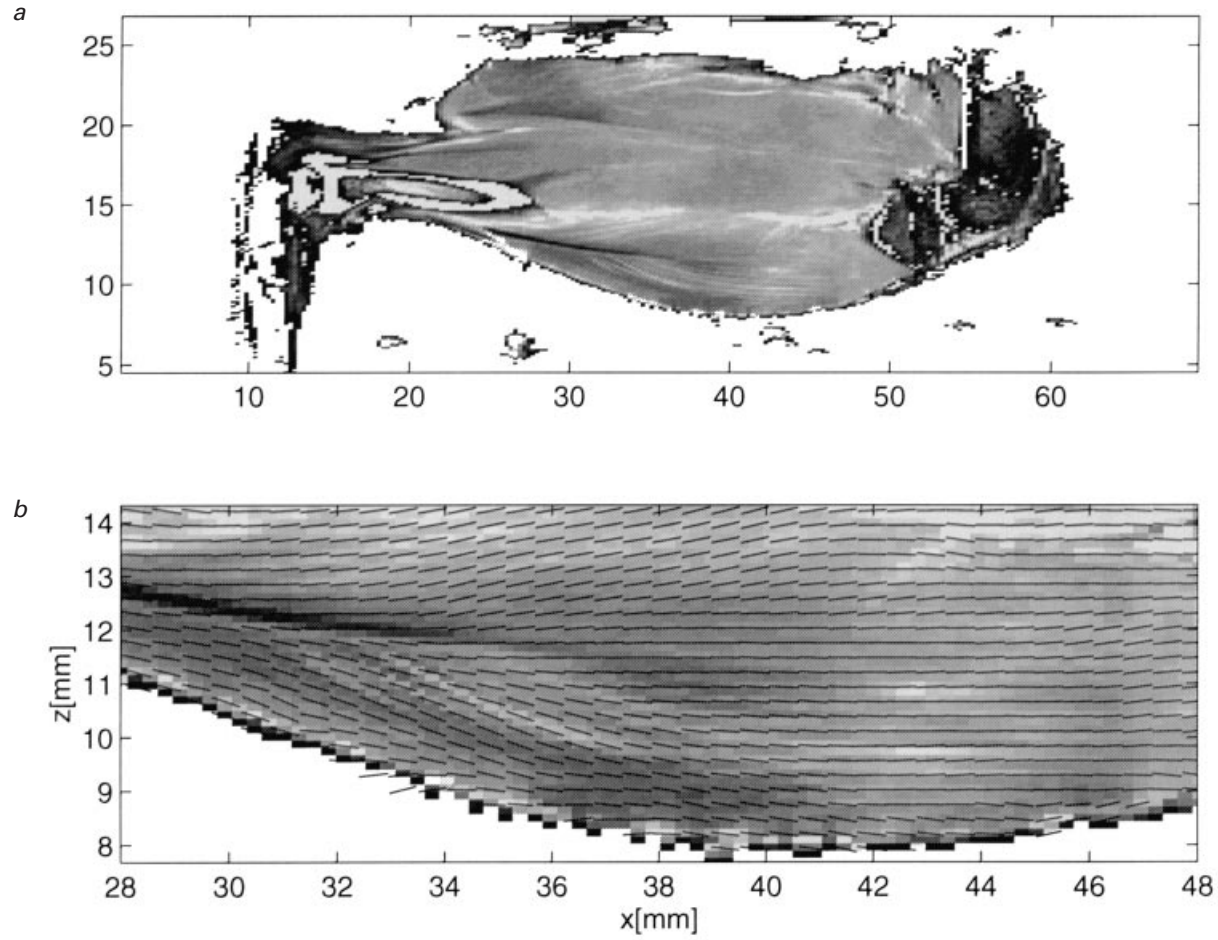

Fig. 3. (*a*) High resolution image HRS-9 through the midsagittal plane of the TA (orientation: left: distal, bottom: ventral). Note the pennate insertion of the muscle fascicles (faint striations) on the dark distal aponeurosis ((26, 13) to (36, 11)). (*b*) Enlargement of HRS-9 of the area around the aponeurosis with a superimposed projection of DTI-9 directions (direction in each voxel based on averaged apparent diffusions of 10 voxels).

Table 1. *The 3 principle diffusion coefficients and quantities derived from the data, in the distributed (per cluster of voxels) and in the proximal region of interest*

	Distributed ROI	Proximal ROI	Hsu et al. (1998)	Van Doorn et al. (1996)	Basser et al. (1994*b*)		Cleveland et al. (1976)
					15 °C	15.5 °C	
λ_1	1.25±0.08	1.17±0.38	0.94±0.28	1.37±0.31	1.078	1.053	1.39
λ_2	0.91±0.10	0.84±0.27	0.74±0.27	—	0.949	0.948	—
λ_3	0.75±0.09	0.70±0.23	0.63±0.24	0.93±0.31	0.836	0.893	1.0
λ_1/λ_3	1.67	1.67	1.49	1.47	1.29	1.18	1.39
Trace	2.91	2.71	2.31	—	2.836	2.894	—

Values (mean±S.D.) in 10^{-9} m² s^{-1}. These data are compared with those found in other studies (Van Doorn et al. (1996): measurement of formalin fixed cat semimembranosus muscle at 20 °C; Basser et al. (1994*b*): measurement of pork loin at 15 °C (left column) and 15.5 °C (right column); Cleveland et al. (1976): nonfixated TA of mature male rat, 10 min to 24 h after dissection, 25 °C.

these effective voxel sizes are essential in the determination of an appropriate voxel size for the FE mesh. They are plotted as a function of effective voxel size in Figure 4. A least squares fit for the hypothetical decrease of the S.D. of DTI direction (α) with the square root of the voxel size (s) yielded $\mathrm{sd}(\alpha) = c{*}s^{-0.5}$, with $c = 4.76°{*}mm^{3/2}$ ($r = 0.86$).

The FE mesh that was created is projected over the

Table 2. *Means and* S.D. (°) *of the proximal and distributed region of interest for the original and averaged data*

	Distributed ROI (DTI-ALS)
Original data (0.09 mm^3)	-2.49 ± 10.48
Averaged 8 voxels (0.72 mm^3)	-3.16 ± 5.28 ($P < 0.01$)
Averaged 10 voxels (0.90 mm^3)	-1.11 ± 3.12
Averaged 12 voxels (1.08 mm^3)	-1.90 ± 3.14 ($P < 0.01$)
Averaged 15 voxels (1.35 mm^3)	-1.54 ± 3.16 ($P < 0.05$)
Averaged 25 voxels (2.24 mm^3)	-1.16 ± 3.03 ($P < 0.05$)

The values in the column with data from the distributed region of interest are actual means and S.D. of the difference in angles (°) between local DTI and ALS. The angles in the column for the DTI data in the proximal region of interest were calculated from the formulae: mean = 0.03∗(voxel size) − 1.45 and S.D. = 4.76∗(voxel size)$^{-0.5}$ (see Fig. 4). Thus these result from averaging different voxels. For significant differences between DTI and ALS, the significance ($P < 0.01$ or $P < 0.05$) is added to the table.

HRS-9 image in Figure 5*a*. In Figure 5*b*, the fibre direction as determined from the appropriate voxel size is shown per element. Proximally and distally thick lines indicate the sites where the muscle is fixed to the tibia and the first metacarpal bone. The corresponding nodes are fixed during the FE simulation. Material and contraction properties are similar to those used by Vankan et al. (1997) for the medial gastrocnemius muscle. An 800 ms tetanic contraction of 100 kPa muscle tension is computed. Calculated deformation just prior to the relaxation is shown in Figure 5*c*.

DISCUSSION

The high resolution images show a high contrast between fat, bone, aponeurosis and muscle. A large part of HRS-9 shows muscle fascicle direction in the high resolution image (Fig. 3*a*). This is agreement with the findings of Scott et al. (1993). The striking resemblance between the projection of the DTI-9 fibre direction averaged over 10 voxels and the fascicle orientation in HRS-9 is evident (see Fig. 3*b*). The

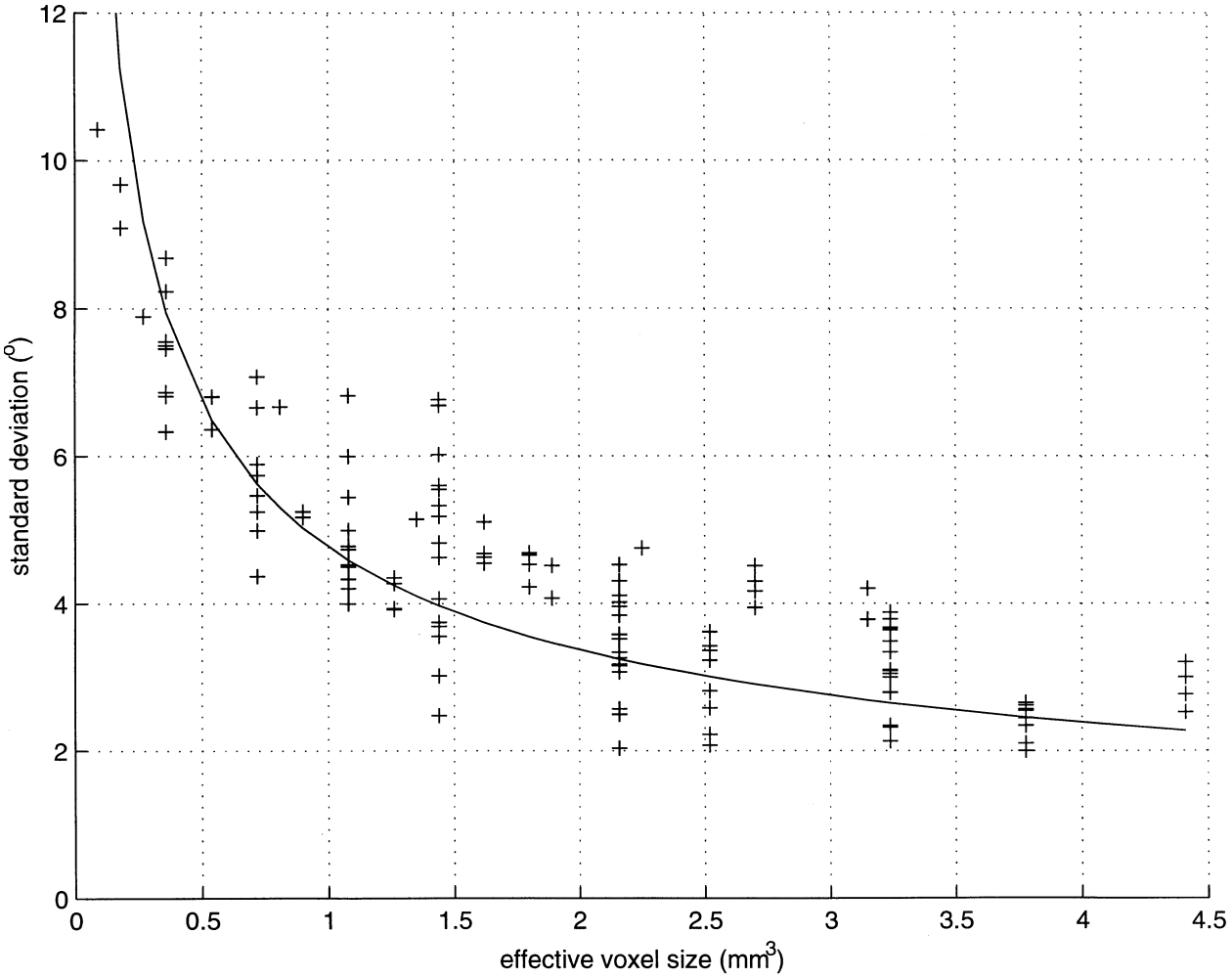

Fig. 4. Standard deviations of DTI angles α (°) with different effective voxel sizes s (mm) in the proximal region of interest. The solid line represents the best fit through these data, using the function S.D. = c∗s$^{-0.5}$, in which c = 4.76° × mm$^{\frac{3}{2}}$. Unlike the mean angle (-1.39 ± 0.99)°, the S.D. strongly depends on voxel size.

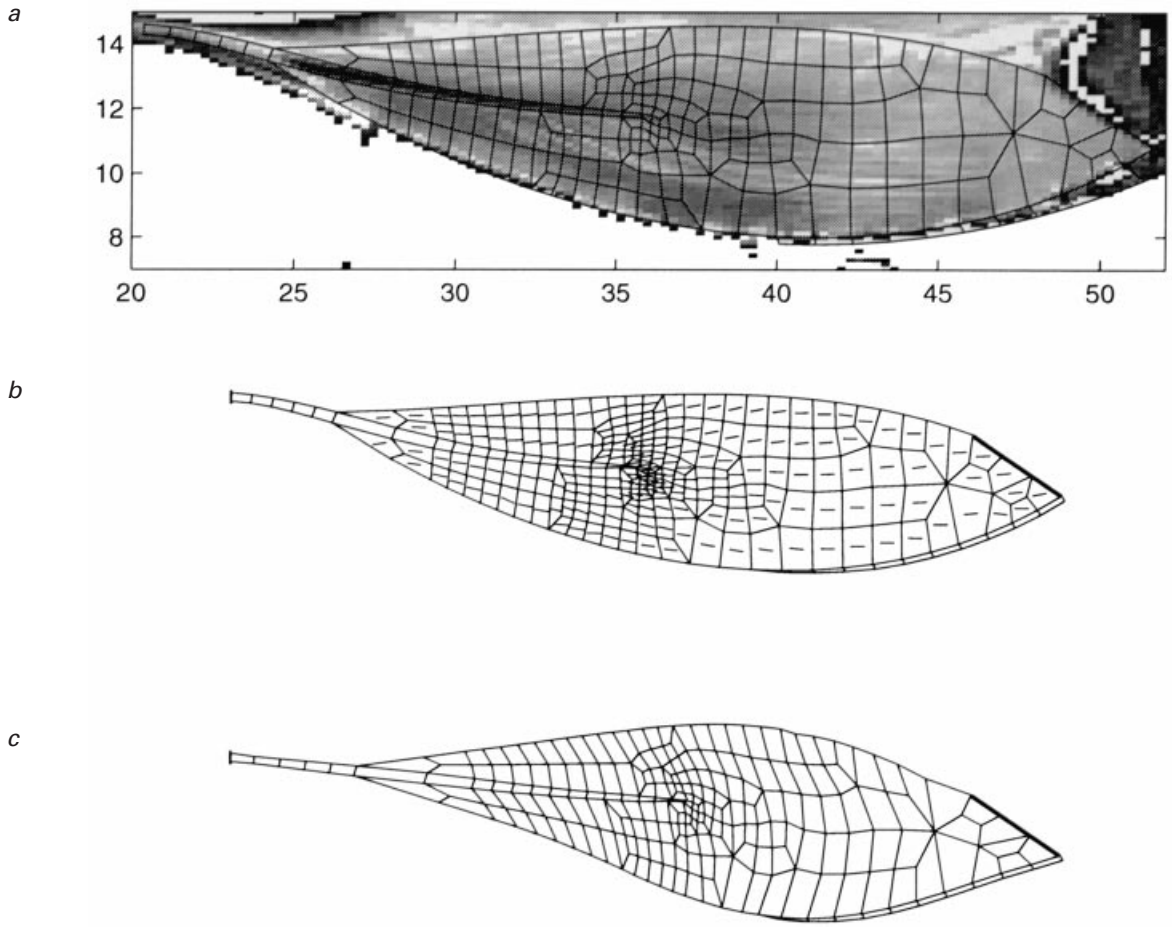

Fig. 5. (*a*) The finite element mesh, created on the basis of MRI experiments, plotted over the HRS-9 high resolution image. (*b*) The fibre directions per element were obtained from DTI data that were calculated from averaged diffusion tensors over 10 voxels. The elements that have no fibre direction indicated represent the proximal and distal aponeuroses. Those are irrelevant with respect to the fibre direction measurements. (*c*) The calculated deformed geometry of the TA muscle during a 100 kPa isometric contraction.

same holds for other planes of the TA. It can therefore be concluded that the qualitative agreement between DTI fibre directions and HRS fascicle orientations is very good.

The DTI directions in the proximal region of interest do not differ from the ALS fibre directions ($P > 0.1$ for all effective voxel sizes). However, in the distributed region of interest, DTI angles are significantly different from ALS angles ($P < 0.05$) for larger effective voxel sizes (Table 2). Probably, in-plane gradients in fibre directions cannot be measured accurately with larger voxels. These gradients are present in the distributed region of interest, but not in the proximal one. More likely however, the approximate 1.7° difference between DTI and ALS both in the proximal and distributed regions of interest result from a misalignment between ALS and the DTI-9 slice. A slight misalignment was determined from the external reference marks due to loss of material during the sawing procedure. As a result, fibre angle gradients affect the comparison between ALS and DTI. This effect is strengthened by the fact that ALS is determined from the surface of the sawing plane, whereas DTI fibre directions are volume-averaged quantities. Other translations and rotations of ALS with respect to MR images have also been considered. A small ($< 2°$) rotation around the z axis exists, which is calculated not to affect the final fibre direction measurements.

Based on the perfect agreement between HRS and DTI and in view of this discussion regarding differences between ALS and DTI, it can be concluded that DTI does indeed measure skeletal muscle fibre directions in fixated skeletal muscle.

The appropriate voxel size has been determined from the relationship between effective voxel size s and the S.D. of DTI angle α. For basic statistical considerations this relationship has been described using the function of $sd(\alpha) = c*s^{-0.5}$. Since 2° variation in ALS is included in the measurement, the calculated relationship is a slight overestimation of the actual standard deviation. The voxel size with 5.0° standard

deviation is 0.9 mm^3, which equals 10 times the original voxel size (Fig. 4). The fibre directions shown in Figure 3, based on this voxel size, nicely follow the HRS-9 fascicle directions. Regarding this procedure it should be kept in mind that accuracy increases but resolution decreases with larger voxel sizes. The ideal voxel size for measurements of fibre directions will therefore depend on actually present gradients in fibre direction and on the aim of the study. In the present data set, the strong fibre direction transition over the distal aponeurosis obviously remains. Even so, pennation angle on the distal aponeurosis is underestimated as a result of the averaging procedure.

The presented relationship between effective voxel size and DTI angle is obtained for formalin fixed skeletal muscle and depends on environmental variables such as temperature (20 °C in our study) and the parameters of the MR experiment, notably the signal to noise ratio in the images. Therefore, the appropriate voxel size cannot be ported directly to other experiments. However, a criterion such as the one used in the present study can be used in all experimental conditions.

The obtained DTI muscle fibre directions are appropriate for inclusion in FE simulations of contracting skeletal muscle, as the presented simulation shows. The FE mesh that was used in this simulation was obtained from high resolution MR images of the same muscle. This illustrates the potential of MR imaging techniques in biomechanical research on skeletal muscle function. This potential is even greater as the calculated deformation could in principle be combined with, for instance, tagging MRI.

Conclusion

It is concluded that DTI directions actually represent local muscle fibre directions in the rat TA muscle. DTI fibre directions resemble fascicle directions visible in high resolution images very well and specific features such as the pennate insertion on the distal aponeurosis are clearly present. The quantitative analysis indicates good analogies between DTI and ALS, although the correlation was not as obvious as was found for cardiac muscle (Hsu et al. 1988). Possible reasons for this have been discussed.

DTI fibre directions can be used directly in numerical simulations of skeletal muscle contractions, provided the variation in fibre directions is acceptable. An appropriate voxel size, providing S.D.S. in angle below 5°, was determined for the current data set after the experiment (0.9 mm^3). It was shown that from the combination of high resolution MR images and DTI measurements, accurate FE meshes could be generated. This shows the potential of MR techniques in biomechanical research on skeletal muscle function.

ACKNOWLEDGEMENTS

A. van Doorn is gratefully acknowledged for his help in the initiation of the DTI studies, S. Gielen for his help in generating the finite element mesh and G. van Vliet for his expert technical assistance during the MRI experiments.

REFERENCES

BASSER PJ, MATTIELLO J, LEBIHAN D (1994*a*) Estimation of the effective self-diffusion tensor from the NMR spin echo. *Journal of Magnetic Research* **103**, 247–254.

BASSER PJ, MATTIELLO J, LEBIHAN D (1994*b*) MR diffusion tensor spectroscopy and imaging. *Biophysical Journal* **66**, 259–267.

BOVENDEERD PH, ARTS T, HUYGHE JM, VAN CAMPEN DH, RENEMAN RS (1992) Dependence of local left ventricular wall mechanics on myocardial fiber orientation: a model study. *Journal of Biomechanics* **25**, 1129–1140.

BOVENDEERD PH, HUYGHE JM, ARTS T, VAN CAMPEN DH, RENEMAN RS (1994) Influence of endocardial-epicardial crossover of muscle fibers on left ventricular wall mechanics. *Journal of Biomechanics* **27**, 941–951.

CLEVELAND GG, CHANG DC, HAZLEWOOD CF, RORSCHACH HE (1976) Nuclear magnetic measurement of skeletal muscle. *Biophysical Journal* **16**, 1043–1053.

COREMANS J, LUYPAERT R, VERHELLE F, STADNIK T, OSTEAUX M (1994) A method for myelin fiber orientation mapping using diffusion-weighted MR images. *Magnetic Resonance Imaging* **12**, 443–454.

ENGSTROM CM, LOEB GE, REID JG, FORREST WJ, AVRUCH L (1991) Morphometry of the human thigh muscles. A comparison between anatomical sections and computer tomographic and magnetic resonance images. *Journal of Anatomy* **176**, 139–156.

GARRIDO L, WEDEEN VJ, KWONG KK, SPENCER UM, KANTOR HL (1994) Anisotropy of water diffusion in the myocardium of the rat. *Circulation Research* **74**, 789–793.

HSU EW, MUZIKANT AL, MATULEVICIUS SA, PENLAND RC, HENRIQUEZ CS (1998) Magnetic resonance myocardial fiber-orientation mapping with direct histological correlation. *American Journal of Physiology* **274**, H1627–H1634.

HUYGHE JM, ARTS T, VAN CAMPEN DH, RENEMAN RS (1992) Porous medium finite element model of the beating left ventricle. *American Journal of Physiology* **262**, H1256–1167.

MCLEAN M, PROTERO J (1992) Determination of relative fiber orientation in heart muscle: methodological problems. *Anatomical Record* **232**, 459–465.

MOSELEY ME, COHEN Y, KUCHARCZYK J, MINTOROVITCH J, ASGARI HS, WENDLAND MF, et al. (1990) Diffusion-weighted MR imaging of anisotropic water diffusion in cat central nervous system. *Radiology* **176**, 439–445.

NAKADA T, MATSUZAWA H (1995) Three-dimensional aniso-

tropy contrast magnetic resonance imaging of the rat nervous system: MR axonography. *Neuroscience Research* **22**, 389–398.

PIERPAOLI C, BASSER PJ (1996) Toward a quantitative assessment of diffusion anisotropy. *Magnetic Resonance Medicine* **36**, 893–906.

REESE TG, WEISSKOFF RM, SMITH RN, ROSEN BR, DINSMORE RE, WEDEEN VJ (1995) Imaging myocardial fiber architecture in vivo with magnetic resonance. *Magnetic Resonance Medicine* **34**, 786–791.

SCOTT SH, ENGSTROM CM, LOEB GE (1993) Morphometry of human thigh muscles. Determination of fascicle architecture by magnetic resonance imaging. *Journal of Anatomy* **182**, 249–257.

STEJSKAL EO, TANNER JE (1965) Spin diffusion measurements: spin echos in the presence of a time-dependent field gradient. *Journal of Chemical Physics* **42**, 288–292.

VAN DOORN A, BOVENDEERD PH, NICOLAY K, DROST MR, JANSSEN JD (1996) Determination of muscle fibre orientation using Diffusion-Weighted MRI. *European Journal of Morphology* **34**, 5–10.

VAN LEEUWEN JL, SPOOR CW (1992) Modelling mechanically stable muscle architectures. *Philosophical Transactions of the Royal Society of London B, Biological Sciences* **336**, 275–292.

VANKAN WJ, HUYGHE JM, JANSSEN JD, HUSON A (1996) A 3-D finite element model of blood perfused rat gastrocnemius medialis muscle. *European Journal of Morphology* **34**, 19–24.

VANKAN WJ, HUYGHE TM, SLAAF DW, DONKELAAR CCV, DROST MR, JANSSEN JD et al. (1997) Finite element simulation of blood perfusion in muscle tissue during compression and sustained contraction. *American Journal of Physiology* **273**, H1587–H1594.

VANKAN WJ, HUYGHE JM, VAN DONKELAAR CC, DROST MR, JANSSEN JD, HUSON A (1998) Mechanical blood-tissue interaction in contracting muscles: a model study. *Journal of Biomechanics* **31**, 401–409.